Femtosecond optical parametric generators and amplifiers for the near infrared based on BiB_3O_6

Valentin Petrov,[a)] Alexander Gaydardzhiev,[b)] Masood Ghotbi,[a)] Ivailo Nikolov,[b),*]
Ivan Buchvarov,[b)] Pancho Tzankov,[a,**] Frank Noack[a)]

[a]Max-Born-Institute for Nonlinear Optics and Ultrafast Spectroscopy, 2A Max-Born-Str., D-12489 Berlin, Germany;
[b]Department of Physics, Sofia University, 5 James Bourchier Blvd., BG-1164 Sofia, Bulgaria

ABSTRACT

We describe the most relevant optical properties of BiB_3O_6 (BIBO), that make this material an attractive candidate for nonlinear frequency conversion of laser light in general, and down-conversion of femtosecond laser sources operating near 800 nm in particular. Experimental results are presented in the high-energy, low-repetition-rate (1 kHz) regime, demonstrating the unique versatility of BIBO for efficient generation of femtosecond pulses in the infrared up to ~3 μm.

Key words: bismuth triborate, parametric gain bandwidth, femtosecond pulses, optical parametric amplifiers, optical parametric generators, white light continuum generation and amplification, pulse compression

1. INTRODUCTION

Nonlinear optical techniques based on frequency conversion in second-order nonlinear materials offer a highly effective method to expand the spectral range of existing laser sources. Optical parametric generators (OPG) and amplifiers (OPA) are down-conversion devices that can provide widely tunable spectral coverage at longer wavelengths using fixed-frequency laser sources with limited or no intrinsic tuning capability. At the same time, the instantaneous nature of nonlinear gain allows frequency conversion processes to retain the temporal characteristics of the input pump laser, enabling conversion on the femtosecond time scale. This paper is devoted to one particular nonlinear material, bismuth triborate, BiB_3O_6 (BIBO), and more specifically to its unique properties and application potential in frequency conversion of femtosecond laser pulses in the infrared (IR). The femtosecond OPA and OPG experiments described cover the high energy regime with Ti:sapphire amplifiers at a repetition rate of 1 kHz as pump sources. Femtosecond parametric up- and down-conversion using BIBO in the low-energy, high-repetition-rate (56-76 MHz) regime with mode-locked oscillators, demonstrating broad tunability from the UV, throughout the visible, up to ~3000 nm in the IR, has been described elsewhere.[1] Recently BIBO was implemented also in an optical parametric chirped pulse amplifier.[2]

2. BIBO: RELEVANT PROPERTIES

BIBO crystallizes in the noncentrosymmetric monoclinic space group *C*2. Its extraordinarily high, for a borate crystal, second order nonlinearity is in fact due to the $(BiO_4)^{5-}$ anionic groups. Tensor properties, such as the second order nonlinear optical susceptibility, are generally measured and reported in an orthogonal crystallo-physical frame *XYZ* which is fixed to the crystallographic frame *abc* by certain conventions:[3] For monoclinic crystals, $Y \equiv b$ and $Z \equiv c$. For practical applications, however, it is desirable to operate with the contracted nonlinearity tensor d_{il} in the frame of the optical indicatrix or the principal optical axes *xyz*, the same frame in which the phase-matching properties are analyzed. For point group 2 symmetry, one of the principal optical axes (the *x*-axis in BIBO) coincides with the 2-fold symmetry axis *b,* but the position of the other two axes depends both on wavelength and temperature (the *xyz* frame rotates about the *b*-axis). The rotation of the *y*- and *z*-axes with wavelength does not exceed ±1° in the main part of the transparency range of BIBO and has only weak effect on the calculated effective nonlinearity.[3] The temperature dependence is also rather weak, about 0.24° at 1064 nm for a temperature change of 100°C.[4] The measured d_{il} values for BIBO indicate that the deviation from the Kleinman conjecture does not exceed ±10% which equals the experimental error.[3] Assuming that Kleinman symmetry holds and averaging the corresponding values, one arrives at: $d_{14} = d_{25} = d_{36} = 1.66$ pm/V, $d_{11} = 2.53$ pm/V, $d_{12} = d_{26} = 3.2$ pm/V, and $d_{13} = d_{35} = -1.76$ pm/V, with d_{il} defined in the *xyz* frame.[1]

*Current affiliation: LaserLab, ELETTRA, Strada Statale 14-km 163,5 in AREA Science Park, 34012 Basovizza, Trieste, Italy

**Current affiliation: Quantronix Corporation, 41 Research Way, East Setauket, NY 11733, USA

International Conference on Ultrafast and Nonlinear Optics 2009, edited by Solomon Saltiel, Alexander Dreischuh, Ivan Christov, Proc. of SPIE Vol. 7501, 750102 · © 2009 SPIE · CCC code: 0277-786X/09/$18 · doi: 10.1117/12.849179

The expressions for d_{eff} of BIBO in the principal planes have been derived.[1] As usually, θ and φ are the standard polar and azimuthal angles in the *xyz* frame, while the notations "o" and "e" for the ordinary and extraordinary waves, used in a sequence, always follow the convention $\lambda_I\lambda_S\lambda_P$ for the three waves with $\lambda_I \geq \lambda_S > \lambda_P$. For monoclinic crystals, symmetry considerations indicate that only two octants with common principal plane are sufficient to uniquely describe all possible three-wave interactions. However, for down-conversion in BIBO starting from a pump wavelength near 800 nm, it turns out that it is sufficient to consider interactions in the *x-z* plane (φ=0°) only and the first octant ($0 \leq \theta \leq 90°$). In this case $d_{eff} = d_{12} cos\theta$ for ooe, oeo≡eoo interactions and $d_{eff} = d_{14} sin2\theta$ for eeo, eoe≡oee interactions. The angle Ω, which separates the different interaction types in the *x-z* plane, is the angle between each of the two optic axes (defined as directions along which the phase velocity is independent of polarization) and the *z*-axis. Assuming $n_x < n_y < n_z$ for the principal values of the refractive index, BIBO is a positive ($\Omega < 45°$) biaxial crystal and the wavelength dispersion of Ω is more pronounced than that of ϕ. Nevertheless, to derive the expressions for d_{eff}, it is necessary to neglect the dispersion of Ω. The most recent Sellmeier equations of BIBO,[4] valid between 326.3 and 3083 nm, are used in the present paper.

The UV cut-off wavelength in BIBO is 270 nm.[1] At the 1 cm^{-1} absorption level the transmission of BIBO extends from 286 to 2600 nm. The absorption feature near 2400 nm is seen only in thick samples. The same also holds for the OH^- peak near 2800 nm. The transparency of BIBO extends up to 6250 nm, but the practical upper limit is determined by two-phonon absorption. BIBO is in fact one of the crystals offering highest characterized optical quality and homogeneity. The linear losses measured at 1064 nm, are comparable to the losses in high quality KTP, and roughly two times lower than those typically observed in BBO and LBO. The damage threshold of BIBO is above 300 GW/cm^2 for 45 fs long pulses at 800 nm.[1] BIBO is a chemically stable and non-hygroscopic crystal. At present BIBO can be grown by top-seeded growth from stoichiometric melts. Maximum sizes of ~20×20×30 mm^3, ~44×24×10 mm^3, and ~30×30×40 mm^3, and weight of 120 g have been reported in the literature.[1]

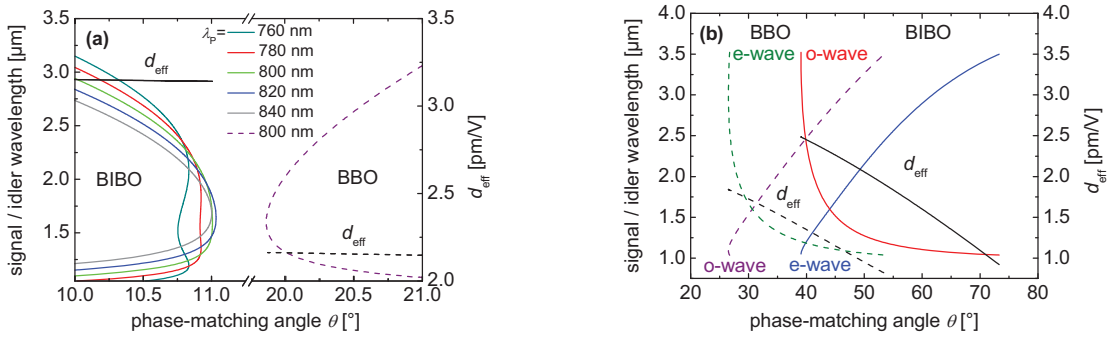

Fig. 1. (a) Down-conversion in BIBO and BBO for negative type-I (ooe) phase-matching at five pump wavelengths near 800 nm. (b) Down-conversion for type-II phase-matching, positive in BIBO and negative in BBO, at a pump wavelength of λ_P=800 nm.

We will compare the properties of BIBO primarily with BBO, which is justified on the femtosecond time scale. Figure 1 shows the important case of OPG or OPA pumped near 800 nm, where regenerative and/or multipass Ti:sapphire laser amplifiers can be used as the pump source. Only ooe type-I phase-matching in the *x-z* plane of BIBO is shown in Fig. 1a, because the eeo type exhibits much lower d_{eff}, whereas Fig. 1b covers both oeo and eoo type-II phase-matching in the *x-z* plane. The phase-matching curves for type-I phase-matching in BIBO cover the full transparency range. After reaching a maximum polar angle (slightly above 11°), the curves change their character of dependence on pump wavelength, and exhibit retracing behavior (two pairs of signal and idler phase-matched simultaneously), which is an indication of broad spectral acceptance (extremely weak dependence on the critical angle). The behavior of BBO is, in principle, similar (shown, for brevity, only for λ_P=800 nm). d_{eff} is almost constant with wavelength in both crystals but much higher in BIBO. In both crystals, type-II phase-matching has two branches (Fig. 1b). In both branches, d_{eff} varies with wavelength, but is always higher for the left branch (oeo in BIBO and eoe in BBO), which alone can cover the entire transparency range with smaller variation of the critical angle θ. In all cases d_{eff} is substantially higher for BIBO than for BBO.

OPG and OPA are travelling-wave type devices which require much higher pump intensities, and hence consideration of the parametric gain bandwidth is desirable. This parameter is proportional to the spectral acceptance but, in addition, takes into account a gain factor. In order to obtain analytical expressions for parametric gain bandwidth, the wave mismatch is usually expanded in series as a function of frequency, assuming in a first approximation that the pump is monochromatic. The individual terms in this expansion are used to evaluate the points, in terms of frequency, where the

gain function, describing the steady state gain for the intensity of the signal wave, in the plane-wave approximation, in the absence of pump depletion, and in the large gain limit, drops to 50% of its maximum value. Analytical expressions can be found in Ref.1. For collinear ooe interaction in BIBO, the first (group-velocity mismatch, GVM) and the third-order term vanish near degeneracy and this makes it necessary to consider the fourth-order term. This is so because approaching degeneracy, when λ_P is close to 800 nm, the second order term (group velocity dispersion, GVD) also vanishes as a consequence of the fact that for polarization parallel to the *y*-axis (o-wave for ooe interaction scheme), it is zero at 1578 nm. It is interesting that the fourth-order approximation should be used for BIBO starting already from ~1500 nm, see Fig. 2a. This approximation predicts a gain bandwidth (FWHM) of about 3800 cm^{-1} (116 THz) near degeneracy. In contrast, the spectral bandwidth of BBO for the same crystal and pump parameters is determined near degeneracy by the GVD and amounts to 63 THz, which is roughly two times smaller, see Fig. 2a.

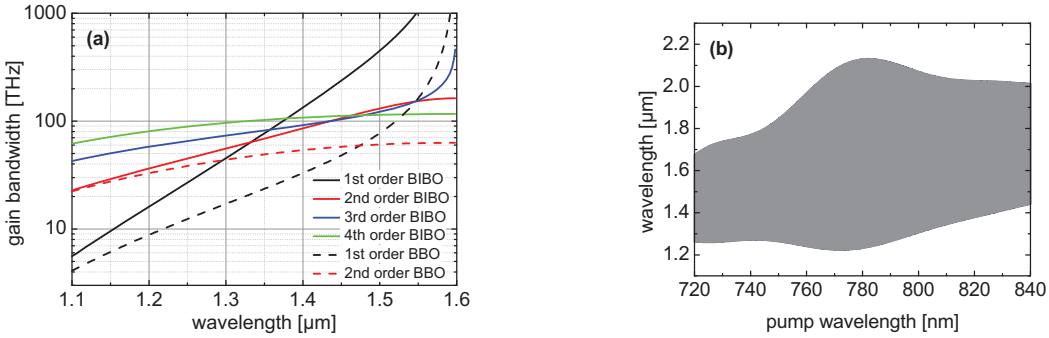

Fig. 2. (a) Gain bandwidth (FWHM) of BIBO and BBO, analytically calculated for collinear type ooe interaction at λ_P=800 nm, a crystal length of 5 mm and pump intensity of 50 GW/cm^2 using only the first, second, third and fourth order Taylor series expansion terms of the wave-vector mismatch Δk, respectively. (b) Gain bandwidth (FWHM) as estimated from numerical calculation. The absolute gain decreases from 1.41×10^8 at λ_P=720 nm to 2.91×10^7 at λ_P=780 nm and to 5.56×10^6 at λ_P=840 nm.

Direct calculations of the parametric gain at the exact phase-matching angle can be performed also numerically. They indicate that the gain bandwidth at first increases but then decreases with the pump wavelength. There exists an optimum pump wavelength near λ_P=780 nm, where the gain bandwidth is maximized. This can be seen in Fig. 2b where the gray area depicts the range limited by the 50% drop in gain from its maximum value. Thus, for λ_P~800 nm, collinear ooe interaction in BIBO is characterized by extremely broad parametric gain bandwidth. Many other nonlinear crystals possess the same property, related to the existence of retracing behaviour of the phase-matching curves but this happens at a certain λ_P which does not necessarily coincide with the wavelengths of the available femtosecond sources that can be used for pumping OPAs or OPGs. As can be seen from Table 1, this same property is also characteristic of periodically-poled materials (Type-0 interaction), where quasi-phase-matching is realized by suitable choice of the poling period. Note that retracing behaviour (and the gain bandwidth) can also be controlled by varying the crystal temperature.

Moreover, there is another favorable property related to the dispersion of BIBO which affects the interaction length with the pump, and consequently the achievable conversion efficiency. The retracing behavior for ooe interaction occurs at angles θ in the vicinity of the phase-matching curve turning point for the inverse process of SHG. Such a turning point (at λ_F) in the dependence of the fundamental wavelength on the phase-matching angle in SHG means nothing but broadband phase-matching, which is equivalent to vanishing GVM between the fundamental and the second harmonic. Indeed, it can be easily shown that this GVM vanishes at the point where $(\partial\theta/\partial\lambda)_{\lambda_F}=0$ for the SHG phase-matching curve. The existence of a turning point is attributed to anomalous dispersion. It, in fact, determines the existence of the retracing phenomenon in the OPA/OPG phase-matching curves. Similar analytical relations cannot be derived for the GVM with the pump in the case of three waves. However, it is clear that an OPA/OPG operating in the vicinity of λ_F will also be characterized by very low GVM between the pump and the other two waves. For example, for ooe interaction in BIBO, the turning point of the SHG phase-matching curve occurs at a fundamental wavelength of λ_F=1637 nm. The calculated λ_F and "magic" λ_P for ultra-broadband parametric amplification are presented in Table 1 for several nonlinear crystals applicable in the near-IR. In the other type-I interaction scheme (eeo) in BIBO, the deviation of λ_F from $2\lambda_P$ is larger and, consequently, the GVM with the pump is also larger. Table 1 shows that the only crystal for which the GVM with the pump at the "magic" pump wavelength is smaller than for ooe BIBO, is CLBO.

Table 1. Parameters of several crystals that can be used in ultra-broadband OPA/OPG schemes pumped below 1 μm: λ_P is the "magic" pump wavelength for which the signal/idler GVD vanishes near degeneracy; λ_F is the fundamental wavelength for broadband SHG, $\Delta\lambda/\Delta\nu$ correspond to the wavelength / frequency range for maximum gain bandwidth calculated at the 1/2 level (crystal length 5 mm, pump intensity 50 GW/cm^2), θ/φ and Λ are the phase-matching angle and the period for degenerate operation at the given λ_P in birefringent and quasi phase-matching, respectively, and the GVM parameter $1/v_P$-$1/v_{S,I}$ is calculated for degenerate operation at λ_P.

Crystal	λ_P [μm]	λ_F [μm]	$\Delta\lambda$ [μm]	$\Delta\nu$ [THz]	θ/φ [°] or Λ [μm]	$1/v_P$-$1/v_{S,I}$ [fs/mm]
KDP (ooe)	0.493	1.035	0.746-1.444	402-208	42.11	14.0
LBO (ooe/eeo) *x-y/x-z*	0.599	1.304	1.043-1.408	288-213	1.35	17.9
CLBO (ooe)	0.627	1.3375	0.987-1.713	304-175	28.57	10.8
BBO (ooe)	0.716	1.541	1.203-1.767	249-170	21.33	15.2
BIBO (ooe) *x-z*	0.789	1.637	1.289-2.032	233-148	10.97	11.9
BIBO (eeo) *x-z*	0.810	1.794	1.237-2.345	243-128	35.11	31.5
PPSLT (eee)	0.825	2.378	1.486-1.856	202-162	21.56	189
PPKTP (eee)	0.895	2.503	1.471-2.286	204-131	32.54	141
$LiNbO_3$ (ooe)	0.949	2.028	1.624-2.284	185-131	46.27	37.2
PPLN (eee)	0.957	2.699	1.647-2.272	182-132	27.93	161
$KNbO_3$ (ooe) *x-y*	0.988	2.138	1.665-2.442	180-123	47.71	46.3
$KNbO_3$ (ooe) *y-z*	1.004	2.066	1.681-2.497	178-120	15.63	17.8
$LiIO_3$ (ooe)	1.040	2.235	1.784-2.488	168-107	20.13	16.0

Similar arguments also hold for quasi-phase-matched materials, where the turning point is defined with respect to the phase-matching period. Since, in this case, the polarization of the three waves is the same, one can expect the deviation of λ_F from $2\lambda_P$ to be larger, leading to larger GVM with the pump. For instance, the GVM with the pump in the degenerate PPKTP-OPA pumped at the "magic" wavelength amounts to 141 fs/mm, in PPSLT it is as high as 189 fs/mm, while it is only 11.9 fs/mm in BIBO (ooe).

It should be emphasized that the "uniqueness" of the dispersive properties of BIBO with respect to the achievable gain bandwidths originates from the fact that in comparison to existing crystals, it exhibits these important properties in collinear interaction, at a pump wavelength coinciding with the most widely used and technologically developed ultrafast Ti:sapphire laser amplifiers, which are routinely deployed as pumps for femtosecond OPAs/OPGs. As a result of the specific behavior of its three refractive indices (presumably related to anomalous infrared dispersion), the two characteristic wavelengths, λ_F and $2\lambda_P$, in BIBO are very close, especially for type ooe phase-matching, leading to low GVM among all the three waves in a degenerate OPA/OPG pumped near 800 nm.

3. FEMTOSECOND OPGs AND OPAs PUMPED NEAR 800 nm

Here, we present experimental results on one- and two-stage OPAs based on different combinations of BIBO crystals (type-I and type-II), seeded by white-light continuum (WLC) or unseeded (OPG), in which the process is initiated by parametric fluorescence. These devices operate at 1 kHz and deliver high energy tunable femtosecond pulses.

3.1 Broadly tunable type-II BIBO OPA

Many femtosecond applications generally require broad tunability. Although several different system configurations have been exploited in the past, at present the material of choice for use in near-IR OPG/OPAs with 800 nm pumping, is type-II BBO. This is due mainly to the possibility to tune, even close to degeneracy, with almost constant signal and idler spectral bandwidth. The same holds for oeo type-II interaction in BIBO, with the advantage of offering higher d_{eff}. The nonlinear figure of merit which enters the exponential gain, FM= $d_{eff}^2 / n_P n_S n_I$, is roughly two times higher than that of BBO, and changes by less than ±10% across the whole tuning range (Fig. 1b).

We compared type-II BIBO and BBO in the double pass OPA shown in Fig. 3a, seeded by WLC which is generated in a 2-mm-thick sapphire plate. A polarizer between the two passes through the nonlinear crystal serves to select the signal wavelength for seeding the second pass, pumped by ~300 μJ. Using a 5-mm-thick AR-coated BBO crystal, sub-200 fs pulses were generated, tunable from 1180 to 2500 nm, with a maximum output level of 80 μJ (signal plus idler) for a total pump energy of 375 μJ. Such overall conversion efficiencies (on the order of 20%) are typical for type-II BBO.

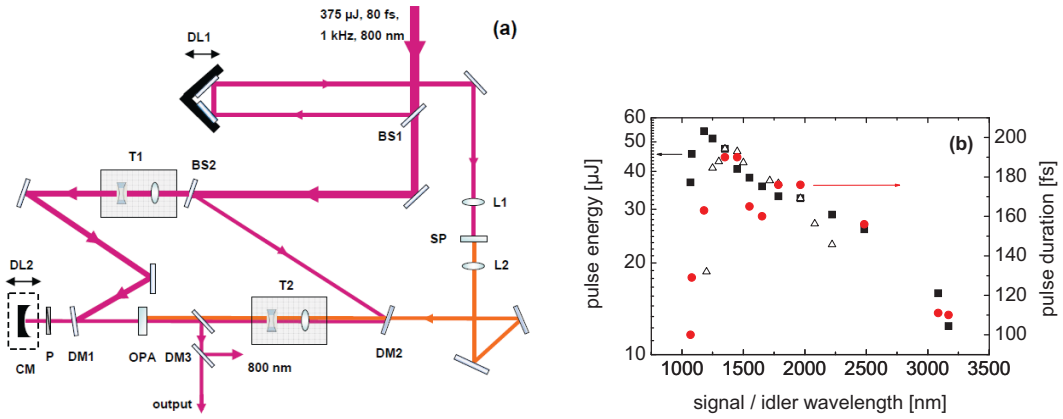

Fig. 3. (a) Experimental set-up of the WLC-seeded type-II OPA: L, lenses, T, telescopes, BS, beam splitters, DM, dichroic mirrors, DL. delay lines, SP, sapphire plate, CM, curved mirror with 30 cm radius of curvature. (b) Pulse energy (full squares) and pulse duration (FWHM) assuming Gaussian pulse shapes (full circles) for the BIBO based OPA using a 3-mm thick sample. The open triangles show the energy obtained with an AR-coated 5-mm thick BBO crystal.

With a 3-mm-thick BIBO crystal, cut at θ=42° in the *x*-*z* optical plane, similar pulse durations were achieved throughout the whole tuning range, which, however, extended slightly beyond 3000 nm, Fig. 3b. Although the maximum energy was on the same order of magnitude, the internal conversion efficiency was clearly higher (more than 30% at maximum for the second pass), because the BIBO sample was uncoated. Shorter BIBO crystal had to be used in type-II interaction in order to have comparable gain bandwidth. This somewhat diminishes the advantage of the higher effective nonlinearity. Nevertheless, the use of a shorter crystal helps to avoid undesirable higher-order nonlinear processes and to better utilize the transparency window of the material, reaching longer idler wavelengths in particular. Thus, e.g. at 3050 nm, an idler pulse duration of 110 fs is obtained. The time-bandwidth product of $\tau\Delta\nu$=0.55 is somewhat above the Fourier limit of 0.44 for Gaussian pulses. The pulses at the corresponding signal wave (1085 nm) are slightly shorter (100 fs).

3.2 High energy type-II / type-I BIBO OPA

Enhancement of output energy from an OPA clearly requires more flexibility on the pumping conditions for the two stages and their separation. A well-known concept in multistage amplifiers is to define the spectral properties and tune the wavelength through the first stage, then use a broadband amplifier in the second stage. This can be realized using a type-II BIBO crystal in the first and a type-I BIBO crystal in the second stage. Note that ooe type-I phase-matching in BIBO is characterized by higher (≈1.3 times) d_{eff} than oeo type-II interaction, which is also almost constant (<3% variation) across the whole tuning range, see Fig. 1a.

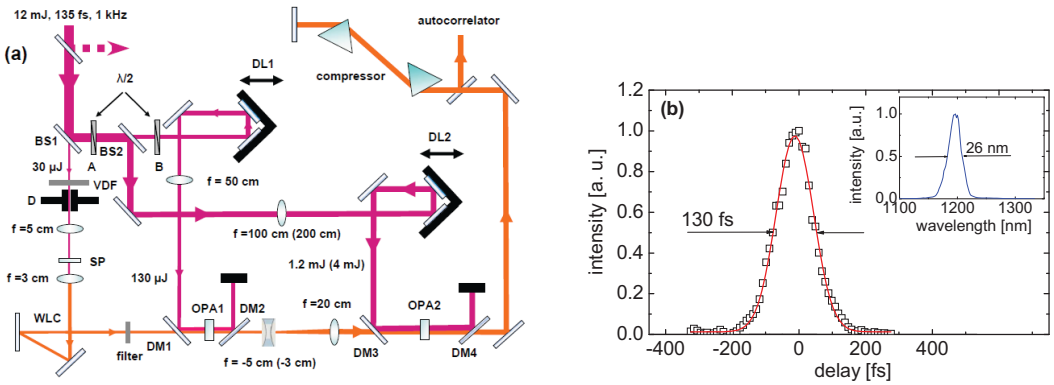

Fig. 4. (a) Schematic of the experimental set-up: OPA1 and OPA2, first and second OPA stages, BS, beam splitters, DL, delay lines, D, diaphragm, VDF, variable density filter, SP, sapphire plate, DM, dichroic mirrors. The values in brackets refer to the high-power version; A and B denote two possible positions of the same half-wave plate (λ/2). (b) Autocorrelation trace (symbols) and Gaussian fit (curve) of the compressed signal pulse at 1200 nm from the low-power OPA. The inset shows the corresponding spectrum.

The high-power OPA, Fig. 4a, is pumped by 5 of the available 12 mJ from a Ti:sapphire amplifier, limited by the available aperture of the nonlinear crystals. The pump pulse duration is 135 fs (Gaussian shape assumed). The central wavelength of the pump pulses was near 807 nm and their spectral width corresponded to a time-bandwidth product of 0.62. A small part of the fundamental pulse energy is used for WLC generation. The Stokes spectral portion of the WLC, for seeding the first OPA stage at the signal wavelength, is selected using a thin long-pass filter (Fig. 4a). The main part of the fundamental power is divided further into two parts for pumping the two OPA stages. In the first stage we employed the 3-mm-thick type-II BIBO crystal described in the previous sub-section. The type-I BIBO crystal in the second stage was 6-mm-thick, also uncoated, with an aperture of 10×10 mm^2. It was cut at θ=11.4° in the x-z principal plane. The output of the first OPA stage (signal plus idler) amounted to several μJ, depending on wavelength. The second BIBO crystal was placed about 45 cm away from the first stage. Without any additional polarization elements, it could be seeded either only by the amplified signal or only by the generated idler in the first stage. This is a consequence of the fact that different types of interaction are used in the two stages.

Initially, we attempted seeding at the signal wavelength. In this case, the half-wave plate (Fig. 4a) is in position A in order to rotate the pump polarization from horizontal to vertical, that is perpendicular to the polarization of the WLC, for both OPA stages. In the low energy regime of this experiment, the second OPA stage was pumped by 1.3 mJ and the pump beam was loosely focused by an f=100 cm lens (Fig. 4a). The spot size resulted in a peak axial intensity of ≈25 GW/cm^2. The maximum output energy (signal plus idler) was about 350 μJ near λ_S=1200 nm, decreased to about 300 μJ at shorter wavelengths (λ_S=1170 nm) and to 260 μJ close to degeneracy. Thus, the maximum conversion efficiency for this stage was about 27%, or ≈34% intrinsic efficiency, taking into account that the crystal is uncoated. We characterized the low-power mode of operation at two signal wavelengths: λ_S=1200 and 1400 nm. At λ_S=1400 nm, the wavelength dependence of parametric gain bandwidth is only weakly pronounced for both stages. In comparison to operation near λ_S=1200 nm, the spectral acceptance is narrower for the first stage and broader for the second stage. Near 1200 nm, the shortest pulses obtained directly from the OPA were 105 fs (FWHM, assuming Gaussian pulse shapes), roughly 20% shorter than the pump pulses, and the spectral width (26 nm) resulted in a time-bandwidth product of $\tau\Delta\nu$=0.57, very similar to that of the pump pulses. Applying the prism compressor, consisting of two 59° SF11 prisms, we were able to shorten the signal pulses down to 92 fs, which resulted in improvement of the time-bandwidth product down to $\tau\Delta\nu$=0.5, see Fig. 4b. The performance of the OPA at λ_S=1400 nm was very similar. Given the modest compression factors achieved, we did not implement the compressor in the high-power regime.

In order to study the potential for energy scaling, the pump energy for the second stage was increased to 4 mJ. Exchanging the beam splitters, it was possible to preserve the same pumping conditions for the WLC and the first OPA stage. The pump beam completely filled the aperture of the BIBO crystal used in the second OPA stage and the peak on-axis pump intensity was ~40 GW/cm^2. By continuing to seed with the signal from the first stage, the maximum energy obtained from the second OPA stage reached 1.1 mJ (signal plus idler) near λ_S=1200 nm. The signal spectra had a short-wave shoulder, and the autocorrelation traces indicated the presence of satellite pulses and/or a longer pedestal, a consequence of simultaneous direct seeding of the second OPA stage by the WLC. This effect was absent only in the limits of the tuning range, for λ_S approaching 1100 nm, where the total output energy (signal plus idler) amounted to 1 mJ, corresponding to an intrinsic conversion efficiency of ≈32% for the second stage. The deconvolved signal pulse duration, assuming Gaussian pulse shape, was ~140 fs (FWHM), resulting in a time-bandwidth product of $\tau\Delta\nu$=0.85. At longer λ_S, the contribution of the direct seed from the WLC stage continuously increased and near 1300 nm it became the main factor in determining the output energy from the second OPA stage. In the high-power regime, it was not possible to eliminate this effect by modifying the imaging of the WLC and the seed from the first stage, because of the large gain bandwidth of the second stage. The problem was solved by seeding the second OPA stage only by the idler generated in the first stage. This was realized by simple translation of the half-wave plate to position B in Fig. 4a, and rotation of the ooe type-I BIBO crystal by 90°. Thus, the WLC has the same extraordinary polarization (in the horizontal plane) as the pump for the second stage, and no phase-matching is possible. In general, seeding at λ_I produced an energy output which was roughly 80% of the total output when seeding at λ_S. Thus, near λ_S=1200 nm, the total output energy when seeding with the idler from the first OPA stage amounted to 850 μJ. Towards degeneracy the energy declined to ~600 μJ. The spectra for two signal-idler pairs are shown in Fig. 5a and the corresponding autocorrelation traces can be seen in Fig. 5b. The latter were well-fitted by Gaussian profiles. The resulting pulse durations were almost constant, varying only from 133 to 139 fs, that is very close to the pump pulse duration. The time-bandwidth products near degeneracy (see Fig. 5b) were also very close to the product for the pump pulses, but away from degeneracy they were slightly larger. The values correspond to roughly 1.5-2 times the Fourier limit for Gaussian pulses.

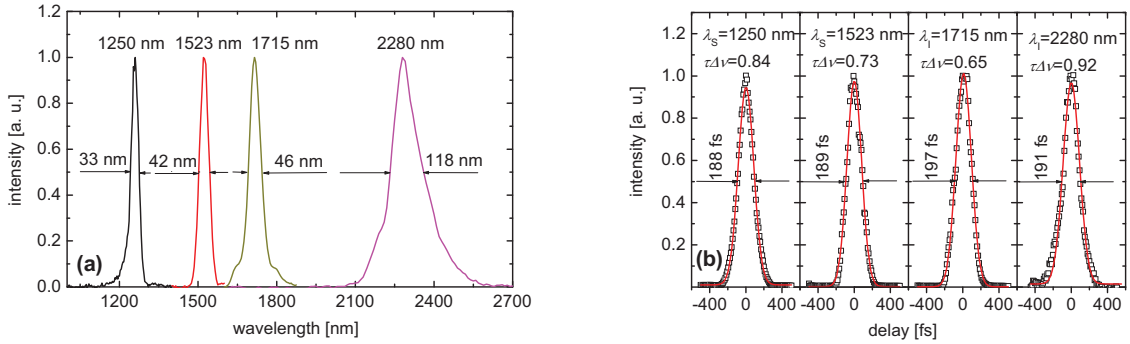

Fig. 5. (a) Spectra of the high-power OPA with idler seeding, recorded for two signal-idler pairs at total output energy of 600 μJ (near degeneracy) and 800 μJ (away from degeneracy). (b) Autocorrelation traces (symbols) and Gaussian fits (curves) with FWHM for the signal and idler pulses, corresponding to the spectra from (a). The time-bandwidth products are also given in the figure.

3.3 High power sub-30 fs pulses with type-I / type-I BIBO OPA

Extremely short high energy laser pulses in the near-IR are of special interest for a variety of applications in nonlinear optics and time-domain spectroscopy. BBO has been widely used before but the analysis of the dispersion properties in section 2 shows that ooe type-I BIBO is an ideal candidate for obtaining such pulses from an OPA pumped at λ_P~800 nm. Here, we present experimental results using such crystals in both stages of a collinear OPA seeded by WLC. The set-up, shown in Fig. 6a, is similar to that in Fig. 3a, using the same pump source at 807 nm and 1 kHz, adjusted to a pulse duration of ~150 fs. The pump pulse energy is about 1.8 mJ, with ~200 μJ used in the first BIBO stage. The crystals in both stages are 3-mm-thick, uncoated BIBO, cut at θ =11.4° in the *x*-*z* plane. The characterization of the generated signal and idler pulses was performed using SHG frequency-resolved optical gating (SHG FROG) technique.

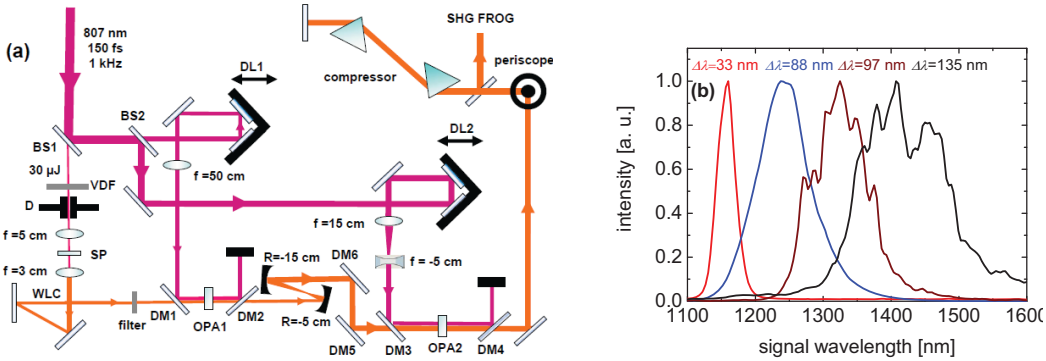

Fig. 6. (a) Schematic of the experimental set-up: OPA1 and OPA2, first and second OPA stages, BS, beam splitters, DL, delay lines, D, diaphragm, VDF, variable density filter, SP, sapphire plate, DM, dichroic mirrors. (b) Typical spectra of the amplified near-IR signal pulses across the tuning range.

Spectral and temporal behavior of the WLC amplified in the first stage strongly depends on λ_S. For 1150 nm<λ_S<1300 nm, well-defined spectra with 30-100 nm bandwidth, increasing with wavelength, and pulse energies exceeding 5 μJ, are achieved. Starting from 70 fs near 1150 nm, the signal pulses become shorter down to 40 fs with increasing wavelength, which is to be expected given the better group velocity matching with the pump. At λ_S>1300 nm, the behavior changes dramatically: Firstly, the WLC energy decreases, and in order to produce sufficient signal energy for seeding the second OPA stage, the pump intensity should be increased by moving the crystal closer to the focal point. Secondly, because of the broader gain bandwidth of BIBO in this range, smooth wavelength tuning is no longer possible and a broad spectrum with limited tunability near ~1400 nm is selected by the crystal. At this wavelength, the negligible GVD of BIBO (~33 fs^2/mm) results in near transform-limited signal pulses as short as ~18 fs without any compression.

For the amplification of the generated signal pulses from the first stage, about 1.6 mJ of pump pulse energy is delivered to the second OPA stage, seeded only at the signal wavelength. The amplified signal pulses in the second stage nearly

follow the behavior of the seed pulses from the first stage: Typical spectra are shown in Fig. 6b. For λ_S<1200 nm, where the GVM still determines the gain bandwidth, the signal spectra are about 30 nm broad. On the other hand, for wavelengths in the 1200 nm<λ_S<1300 nm range, where the parametric gain bandwidth drastically increases, spectral widths of 80-120 nm are obtained for the signal, which support sub-30 fs transform-limited pulses.

Across the tuning range of 1150 nm<λ_S<1300 nm more than 400 μJ (signal plus idler) of pulse energy is produced in the second stage, corresponding to an internal conversion efficiency of 30% in this stage. In order to compress the signal pulses, we applied the same prism pair compressor from the previous sub-section with a separation of 50-70 cm, depending on wavelength. At λ_S=1300 nm, the retrieved pulse duration of 25 fs (FWHM) corresponds to nearly bandwidth-limited pulses (time bandwidth product of $\tau\Delta\nu$=0.31). Unfortunately, such high-energy signal pulses were obtained only over a limited spectral range near 1300 nm. Tuning towards 1400 nm was accompanied with difficulties related to the suppression of the OPG effect and such tuning extension would probably require the addition of an intermediate amplification stage for improved optimization, which would result in increased complexity.

We also measured the idler pulses generated in the second stage in the spectral range characterized by high output energy. At λ_I~2300 nm they were also almost transform limited with a duration of 55 fs and a spectral width of 160 nm ($\tau\Delta\nu$~0.5). Being negatively chirped, the idler pulses cannot be further compressed by a normal prism pair compressor.

3.4 Ultra-broadband WLC amplification in BIBO

The technique commonly used to obtain ultra-broadband (more than an octave) coherent radiation is based on white-light generation in transparent materials using femtosecond lasers, however, the achievable pulse energies of single filament WLC sources at 1 kHz repetition rate are still very low (typically tens of nanojoules). The concept of ultra-broadband coherent amplification (or generation, when starting from parametric super-fluorescence) relies on OPA at achromatic phase-matching condition, defined by zero GVM between idler and signal pulses along the direction of the signal wavevector. For collinear type-I interaction, this condition is always fulfilled near degeneracy ($\lambda_S \approx \lambda_I$), but the bandwidth can be further enhanced if the GVD of the signal and idler waves also vanishes, as in the case of BIBO, see section 2. Here we present results of ultra-broadband collinear OPA in ooe type-I BIBO. Since continua generated from 800 nm exhibit strongly decreasing intensity towards 1600 nm, we used the anti-Stokes part of the WLC generated at longer pump wavelengths as seed (Fig. 7a). The OPA is pumped with 45 fs pulses (Gaussian shape assumed) using about 0.7 mJ of the available 2 mJ of pump energy, distributed among the OPG used to pump the WLC generator (3-mm YAG plate), the pump beam for the BIBO OPA, and the probe beam (Fig. 7a). An additional BBO OPG was used as the pump source for the WLC seed (50 fs idler pulses near 2.1 μm). The single filament WLC was recombined with the pump beam at 800 nm for the BIBO-OPA stage. The uncoated 3- and 5-mm-thick BIBO crystals employed in the OPA were cut at θ=11.4° in the *x*-*z* plane. The average pump intensity (½ of the peak on-axis level) at 800 nm was 60 GW/cm^2. Using a fraction of the fresh pump beam as a gate pulse, XFROG (cross-correlation FROG based on SFG) measurements of the parametrically generated radiation were performed. The latter were used to reconstruct the entire spectrum and the integral pulse duration for the amplified WLC, as well as to obtain rough information about the phase-modulation.

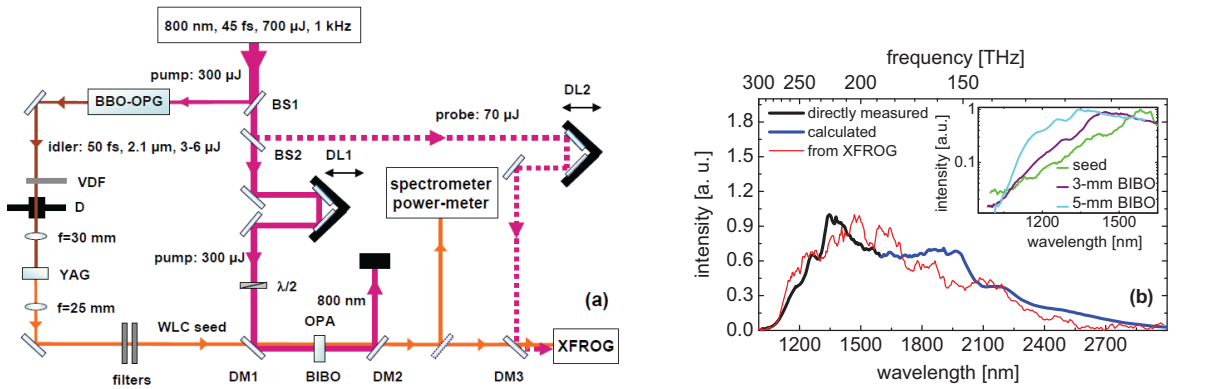

Fig. 7. (a) Schematic of the experimental set-up: BS, beam splitters, DL, delay lines, D, diaphragm, VDF, variable density filter, DM, dichroic mirrors, filters, Ho:YAG mirrors reflecting the 2.1 μm pump. (b) Spectra of the WLC amplified in the 5-mm-thick BIBO: measured by an InGaAs spectrometer (black curve), reconstructed from the time-integrated XFROG trace (thin red curve) and computed from the Manley-Rowe relation (blue curve). The inset is a comparison of the InGaAs measured spectra of the WLC seed generated in YAG (green line), and the amplified WLC in the 3-mm-thick (purple line) and 5-mm-thick (cyan line) BIBO crystals.

Typical energies achieved for the amplified WLC were 30 and 50 μJ for the 3- and 5-mm-thick BIBO crystals, respectively. These values were obtained for pump delays which simultaneously provided ultra-broad bandwidths of the amplified WLC. Thus, the maximum intrinsic conversion efficiency was 20% for the 5-mm-thick BIBO. The amplified WLC spectrum in the case of 5-mm thick BIBO is shown in Fig. 7b. The obtained amplification bandwidth was ~80 THz for the 3-mm-thick BIBO, and it increased to ~100 THz in the case of the 5-mm-thick BIBO. The FWHM of the cross-correlation functions recovered from the XFROG measurement were 84 and 105 fs for the 3- and 5-mm-thick BIBO crystals, respectively, and so the corresponding amplified WLC pulse durations assuming Gaussian pulse shape (FWHM intensity) are ~70 fs and ~95 fs, 1.4 and 1.9 times longer than the pump pulses at 2.1 μm, respectively. The time-bandwidth product, thus, amounts to 5.6 and 9.5 for the 3- and 5-mm-thick BIBO crystals, respectively. The simultaneous increase in the spectral width and pulse duration for the thicker BIBO crystal can only be explained by considering chirp effects. In that case, the increasing temporal walk-off between the pump and amplified pulses results in spectral broadening. The WLC seed level did not allow direct characterization of its temporal and spectral properties. However, from estimates of GVD in all the optical elements used (including the YAG and BIBO crystals), we conclude that the main source of chirp is the BIBO crystal itself. Since the zero GVD is near the 1600 nm degeneracy point, the chirp produced by GVD in BIBO has opposite sign for the signal and idler frequencies. While this satisfies the requirement for energy conservation in the case of OPA pumped by monochromatic pump it is clear that compensation of such chirp in subsequent pulse compression schemes will not be trivial.

3.5 Ultra-broadband WLC generation in BIBO

If BIBO is the main source of chirp in the WLC OPA just described, then similar performance can be expected from the simpler OPG scheme. Hence, we studied the same two BIBO crystals of length 3 and 5 mm, for an incident pump energy of 260 μJ, but without seeding. Most of the measurements were performed at average pump intensity of 100 GW/cm^2 for the 3-mm and 60 GW/cm^2 for the 5-mm-thick sample. The WLC energy was 8 μJ for the 3-mm and 12 μJ for the 5-mm-thick BIBO crystal. With the shorter crystal, it was possible to raise the pump intensity to 150 GW/cm^2 without any detrimental effects which led to an output energy of 15 μJ, equivalent to an internal conversion efficiency of ~7%.

The dependence of OPG spectra on the phase-matching angle is in agreement with theoretical predictions for the parametric gain, which was calculated numerically, by varying θ for fixed λ_P=800 nm. Accordingly, we observed that the actual gain bandwidth can be further increased when the spectral gain profiles for the signal and idler merge. The phase-matching angle for which this happens is slightly lower than the one corresponding to degeneracy (θ~11° for λ_P=800 nm). The broadest parametric gain occurs before the two spectra have completely merged. It extends roughly from 1.15 to 2.4 μm. The additional bandwidth enhancement is up to ~50% compared to the values given in Table 1. In fact, the broadest parametric gain (depending on its definition, that is the acceptable dip in the spectral distribution) does not necessarily occur for the magic pump wavelength: Both λ_P and θ can slightly deviate from the values in Table 1.

The spectral extent of the WLC is slightly larger for the 5-mm-thick BIBO but at the 0-level it is roughly 135 THz for both crystals. Such weak dependence on the gain, which is roughly 200 times higher in the 5-mm BIBO, is expected when the spectral gain bandwidth is determined by higher-order dispersion terms.[1] The opposite chirp in the signal and idler branches is more pronounced with increasing parametric gain (conversion efficiency). The WLC pulse durations, obtained from the integrated cross-correlation functions derived from the XFROG traces under Gaussian shape assumption, are shorter than in the OPA: 63 fs for the 3-mm-thick crystal pumped at 100 GW/cm^2, 73 fs for the 5 mm thick crystal at the same pump level, and 66 fs for the 3-mm-thick BIBO at 150 GW/cm^2. The time-bandwidth products are roughly 10 times above the Fourier limit: $\tau\Delta\nu$~4.2, ~4.7, and ~5 for these three cases. Using longer (100 fs) pump pulses we established that at the same intensity level, the conversion efficiency of the WLC OPG was doubled, both for the 3- and 5-mm-thick BIBO crystals. The other characteristics were very similar. Thus, the integral WLC pulse durations in this case were shorter than the pump pulses.

In order to obtain a more complete picture of the potentially achievable energy level with this technique, we added a second stage to the BIBO OPG using 3-mm-thick crystals in both stages, in a set-up very similar to that depicted in Fig. 6a. The pump system was the same as described in sub-sections 3.2 and 3.3, adjusted to 140 fs pulse duration. The first stage was pumped by 170 μJ, but at tighter focusing to achieve OPG operation. Its output was then amplified in the second stage OPA, pumped with about 800 μJ of pump energy. The mirrors of the all-reflective telescope between the two stages, see Fig. 6a, were modified to a 3:1 configuration in order to reduce the beam cross-section in the second stage and by using metallic mirrors, both signal and idler were applied for seeding the second stage. The telescope for the pump beam to the second stage was also modified by using lenses of f=30 cm and f=-5 cm, in order to similarly reduce its size. XFROG was again used for the characterization of the amplified WLC pulses but since in this case the pump

pulses near 807 nm were longer than the pulse duration of the amplified WLC, we implemented an interference filter in one arm of a SHG autocorrelator to select 80-fs-long gate pulses at 1300 nm with a spectral width (FWHM) of about 40 nm for the SFG process. The gate pulses themselves were measured independently by SHG FROG.

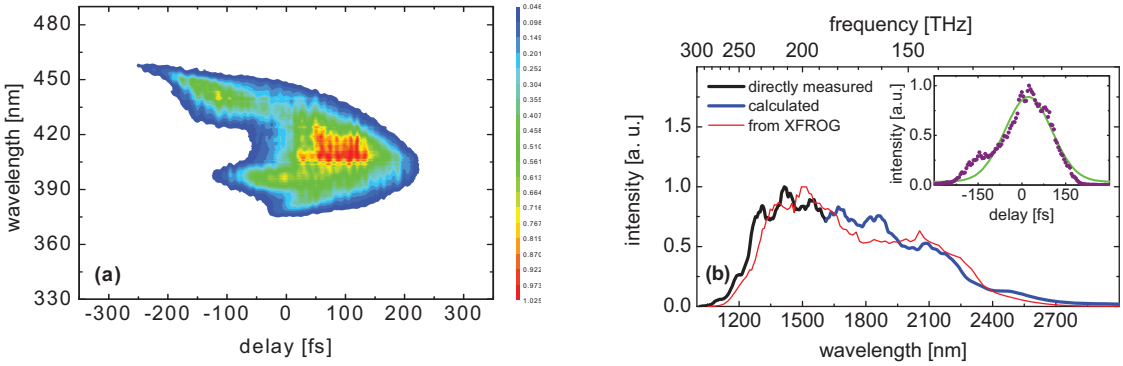

Fig. 8. (a) XFROG trace of the output of the WLC OPG-OPA. (b) Spectra, with notations similar to Fig. 7b. The inset in (b) shows the integrated cross correlation function with Gaussian fit.

Maximum output energy of 115 μJ was obtained from the second stage, thus reaching internal conversion efficiencies close to 17%. In terms of energy, the improvement in comparison to the maximum values obtained with the WLC OPG described before is almost 8-fold. The obtained integral pulse durations were on the order of 170 fs (Fig. 8b). The spectral extension of ~100 THz (FWHM), achieved by alignment of the two stages at slightly different angles, leads to a time bandwidth product of 17, which is 38 times above the Fourier limit for Gaussian pulse shapes. As can be seen from the XROG trace in Fig. 8a, negative chirp is observed above 1600 nm, as well as pronounced positive chirp below degeneracy. Further steps towards compression of the produced amplified WLC employing a scheme with a deformable mirror for simultaneous compensation of both negative and positive chirp are currently under investigation.

4. CONCLUSION

BIBO possesses excellent properties for broadband parametric amplification when pumped near 800 nm in collinear geometry. Higher-order dispersion terms determine then the parametric gain bandwidth, which can be extremely broad, and group velocity matching with the pump ensures long interaction lengths and high efficiency even for femtosecond pulse durations. Hence, BIBO seems predestined for femtosecond down-conversion schemes based on Ti:sapphire lasers and amplifiers as the pump source. We realized several such OPA schemes in the high-power regime at a repetition rate of 1 kHz, demonstrating high conversion efficiency, output energies reaching 1.1 mJ (signal plus idler), tuning extending up to 3000 nm for the idler, sub-30 fs signal and 55 fs idler pulse durations, as well as ultra-broadband near-IR WLC OPAs and OPGs in the sub-100-fs regime, with energy as high as 50 μJ (OPA) and 15 μJ (OPG).

ACKNOWLEDGMENTS

We acknowledge support from DAAD (grant D/07/00333) and Bulgarian Ministry of Science and Education (NSF Grants D01-1174/2007 and VU-L-319/2007)). The research leading to these results has received funding from the European Community's Seventh Framework Programme FP7/2007-2011 under grant agreement n° 224042.

REFERENCES

[1] Petrov, V., Ghotbi, M., Kokabee, O., Esteban-Martin, A., Noack, F., Gaydardzhiev, A., Nikolov, I., Tzankov, P., Buchvarov, I., Miyata, K., Majchrowski, A., Kityk, I. V., Rotermund, F., Michalski, E., and Ebrahim-Zadeh, M., "Femtosecond nonlinear frequency conversion based on BiB_3O_6," Las. & Phot. Rev., DOI10.1002/ lpor.200810075.

[2] Rothhardt, J., Hädrich, S., Limpert, J. and Tünnermann, A., "80 kHz repetition rate high power fiber amplifier flat-top pulses pumped OPCPA based on BIB_3O_6," Opt. Express **17**, 2509-2517 (2009).

[3] Hellwig, H., Liebertz, J. and Bohaty, L., "Linear optical properties of the monoclinic bismuth borate BiB_3O_6," J. Appl. Phys. **88**, 240-244 (2000).

[4] Miyata, K., Umemura, N. and Kato, K., "Phase-matched pure $\chi^{(3)}$ third-harmonic generation in noncentrosymmetric BiB_3O_6," Opt. Lett. **34**, 500-502 (2009).